

A NEW METHOD TO CHARACTERIZE TCO/P CONTACT RESISTANCE IN a-SI SOLAR CELLS

Steven S. Hegedus and Michael Gibson, Institute of Energy Conversion, University of Delaware,
Newark, DE 19716 USA ssh@udel.edu
Gautam Ganguly and Rajeewa Arya, Solarex, Toano, VA 23168 USA

ABSTRACT

A method is presented to characterize the TCO/p contact and the TCO sheet resistance in a-Si based p-i-n superstrate devices. It requires having scribed TCO strips, which are electrically isolated before a-Si deposition, then fabricating rows of individual devices on each strip. Analysis of 4-terminal measurements in different V-sensing configurations yields the TCO/p contact and TCO sheet resistance in a straightforward manner. The method is applied to devices fabricated on 3 brands of commercial SnO₂ substrates. The TCO/p contact resistance is found to be ~2 $\Omega\text{-cm}^2$ and the sheet resistance decreases by 2-4 Ω/sq after a-Si deposition on all 3 brands of SnO₂ substrates.

INTRODUCTION

Transparent conductive oxides (TCO) are critical to the optical and electrical performance of a-Si based solar cells. This is especially true for superstrate a-Si p-i-n solar cells which are deposited on a glass/TCO substrate. Optically, the TCO must have high transparency and provide scattering to enhance light trapping. Electrically, the TCO must have low lateral sheet resistance since there are no grids and low contact resistance with the p-layer. The TCO is subjected to all processing steps including H-rich plasmas during the p-layer deposition which can degrade its optical transparency (1,2). The TCO must be robust, inert to subsequent chemical and thermal device processing (3) and also must be able to be laser scribed with high yield (4). Presently, textured fluorine doped SnO₂ is the standard TCO for commercial applications (5).

Minimizing the resistance between the p-layer and TCO of superstrate p-i-n a-Si devices and modules is a critical issue for utilizing new TCO materials like ZnO and new p-layers like $\mu\text{-SiC}$ or $\mu\text{-SiO}$. Compared to SnO₂, ZnO typically gives higher short circuit density (J_{SC}) due to lower absorption losses but poorer electrical performance (4,6) commonly attributed to the ZnO/p interface, forming a non-ohmic contact. Various schemes to improve the ZnO/p electrical contact have been discussed (7). However, characterization of the TCO/p interface is difficult since it is in series with the dominant p-i-n junction.

We have developed a method to characterize the TCO/p contact based on the work of Shafarman and Phillips (8). This method requires having a two adjacent TCO regions. A device is biased to have standard current flow through its TCO/p contact and TCO region while the voltage is measured on the adjacent TCO pad which is electrically "floating." The second pad is thus a voltage sensing contact giving internal access to the potential in the biased device. An additional benefit to this technique is that the SnO₂ sheet resistance in a completed device structure is also obtained.

SAMPLE FABRICATION

The substrates studied here were textured SnO₂-coated glass made by Asahi Glass (Type U), AFG, or Solarex. The devices were fabricated at Solarex. The SnO₂ on the 3x3 inch square pieces was laser scribed to create long parallel strips approximately 8-10 mm wide and 76 mm (3") long. Then, single junction a-Si p-i-n layers were deposited by PECVD. The p-layers were a-SiC:H. A row of six individual devices were fabricated on each SnO₂ strip by depositing a ZnO/Al back contact (5x5 mm²) mm through a mask on the n-layer. A low resistance contact to the SnO₂ strip was made with Ag paste which was baked at 200°C.

ANALYSIS

A top view and side view of the resulting structure is shown in Figure 1. The two SnO₂ strips of width W, with Ag-paste contacts labeled A and B, each have a row of square devices. The current in cells 1, 2, 3, etc. travels in the SnO₂ a distance L from each device to the SnO₂ contact A. The series resistance of the SnO₂ between the device and the contact is

$$R_{\text{TCO}} = R_{\text{SH}} \times (L/W) \quad (1)$$

where R_{SH} is the sheet resistance of the SnO₂. As L increases, the series resistance of the TCO between the device and its SnO₂ contact increases. Assuming each device is identical, and its TCO/p contact is identical, this increase in R_{TCO} will be the only difference between devices in the same row.

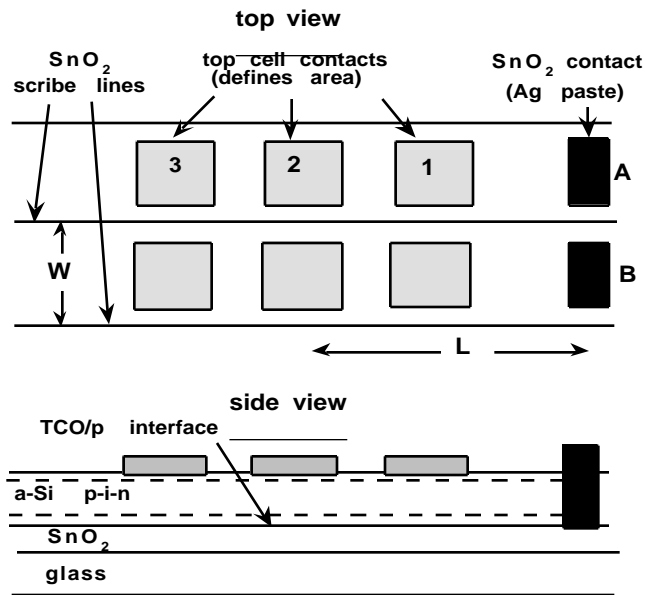


Figure 1. Top view and side view of row of a-Si devices (1-2-3) on scribed SnO₂ strips with contacts labeled A and B.

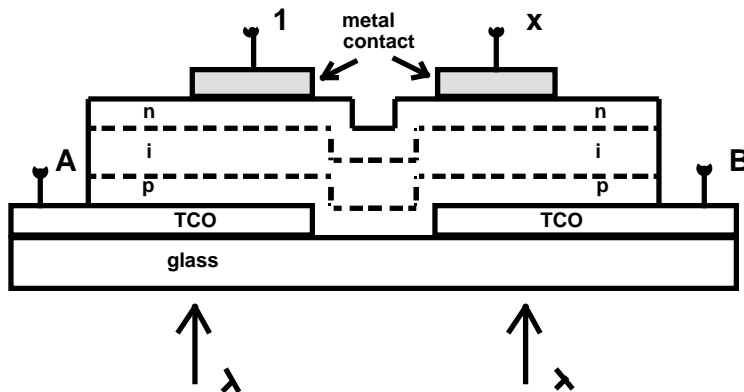


Figure 2. Cross-section view looking down SnO₂ strips A and B. Current flow is established in p-i-n cell 1 between 1 and A while voltage is measured between 1 and A, 1 and B, or A and B. SnO₂ strip B is floating at same potential as the p-layer over strip A.

The three different measurement configurations will be discussed in reference to Figure 2 which shows a cross-sectional view looking down the two SnO₂ strips having contacts A and B. For example, assume that cell 1 in the row of devices labeled 1-2-3 in Figure 1 is to be characterized. For all three measurements, it is biased such that the *current flow* is always between the cell's back contact (1) and the strip's TCO contact (A) as in a standard device JV test. The difference between the 3 measurement configurations is where the *voltage* is measured. In a standard JV measurement, the voltage V_{1A} is measured between the same two contacts where the current is flowing. This voltage V_{1A} includes potential across the p-i-n junction, the TCO/p contact and voltage dropped across the SnO₂ series resistance. When the voltage is instead measured across 1 and B or across A and B, there is no current flow through B so it is floating at the same potential as the p-layer contacting it, i.e. the p-layer over strip A. The SnO₂ strip B is used as a voltage probe giving access to the internal voltage of devices on strip A. Thus, the voltage measured across device 1 and B (V_{1B}) is only the potential *across* the p-i-n junction of a-Si device 1. It excludes the voltage dropped across TCO/p contact and TCO series resistance. Measuring the voltage across adjacent TCO strips (V_{AB}) gives *only* the voltage dropped across TCO/p contact and TCO series resistance since strip B is floating at the same potential as the p-layer above strip A.

We chose to analyze the different JV data in terms of resistances. The three components of resistance and their relation to the three different voltage measurements are given in Equations 2-4. The three dominant resistances are the junction dynamic resistance R_J, the TCO/p contact resistance R_{TCO/p}, and the series resistance through the TCO R_{TCO}, as defined in equation 1. The subscripts 1A, 1B, and AB represent voltage measured between nodes 1 and A, 1 and B or A and B as defined in Figure 2. We assume that the other contact resistances, such as between the cell back contact and the n-layer and between the SnO₂ and Ag contact, are negligible.

$$R_{1A} = dV_{1A}/dJ = R_J + R_{TCO/p} + R_{TCO} \quad (2)$$

$$R_{1B} = dV_{1B}/dJ = R_J \quad (3)$$

$$R_{AB} = dV_{AB}/dJ = R_{TCO/p} + R_{TCO} \quad (4)$$

$$R_J = dV/dJ = (AkT/q)/(J + J_{sc}) \quad (5)$$

A critical assumption is that TCO strip B is floating at the same potential as the p-layer over strip A. If this is correct, equations 2-4 predict that the difference in resistance between cases 1A and 1B should be the same as that measured in case AB. This resistance, R_{AB}, should be the sum of the TCO/p contact and the TCO sheet resistance. From equation 1, R_{AB} should be linear against L/W with a slope of R_{TCO} and an intercept of R_{TCO/p}. Thus, measuring the three resistances on a series of devices on the same strip with increasing L/W should allow determination of R_{TCO/p} and R_{TCO}. Hence, equations 2-4 show two *independent* ways to obtain R_{AB}. This allows verification of the assumptions and the measurements.

RESULTS

Figure 3 shows JV curves for all three cases of voltage measurement on one device (#8090-4C-1) which was on Asahi SnO₂. Normal solar cell JV curves result when the V_{1A} or V_{1B} is measured while V_{AB} gives a linear JV curve through the origin. This linear JV relation indicates the TCO/p contact is ohmic according to equation 4. For purposes of analysis, we determine values of the resistances defined in equations 2-4 at V_{oc}. Thus, for the case where V is measured across 1 and B, R_{oc} is dV_{1B}/dJ at V_{oc}. Values of V_{oc}, FF and R_{oc} are listed in Table I. Note that the V_{oc} is the same between configurations 1A and 1B, as expected since the p-i-n junction determines V_{oc}, but the FF increases in configuration 1B since it excludes the TCO series resistance. V_{oc} is zero in configuration V_{AB} as expected from equation 4. (Some devices we have measured on other TCO materials have exhibited small values of V_{oc} ~20-40 mV in configuration V_{AB}, indicating a photovoltage was developed at the TCO/p contact. These devices had inferior V_{oc} and FF when measured in the standard configuration.)

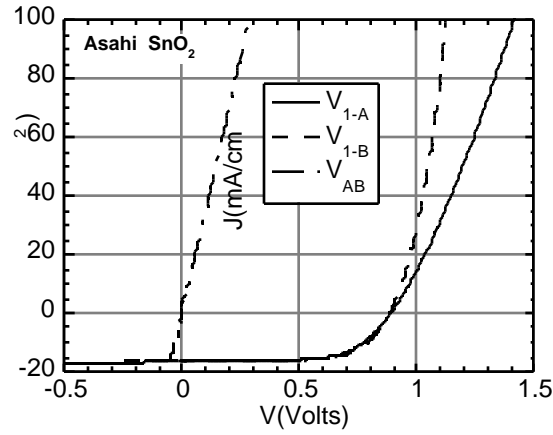


Figure 3. JV curves under illumination for a device (cell 1) with three voltage measurement configurations. Parameters given in Table I.

Table I. FF, resistance at V_{oc} , and V_{oc} for the three curves in Figure 3 obtained from three-voltage measurement configurations on the same device.

test voltage configuration	FF (%)	R_{oc} ($\Omega\text{-cm}^2$)	V_{oc} (V)
cell 1 and A	64	8.8	0.89
cell 1 and B	68	6.1	0.89
A and B	0	2.9	0

Figure 4 shows linear JV behavior for voltages measured across AB for three devices on the same strip of TCO having different L/W. Table II shows values of resistance calculated from both methods. The two resistances increase with L/W as expected, and the FF measured in standard configuration (V_{CELL-A}) decreases as L/W increases as expected. Note the close agreement in Table II between resistances determined independently.

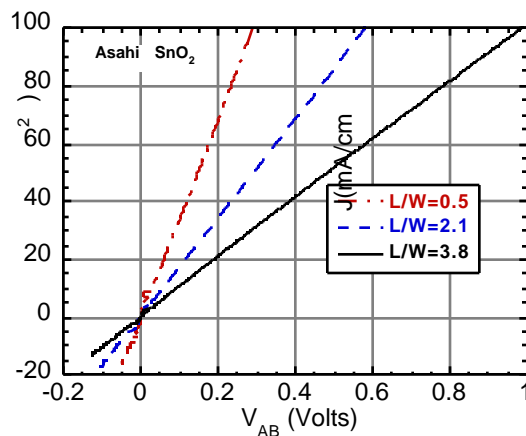


Figure 4. JV measurements for three devices with varying L/W on the same TCO strip A. Voltage was measured across the adjacent strips A and B.

Table II. Resistance and FF for 3 devices with increasing L/W. $R(V_{AB})$ determined from slopes of lines in Figure 4. R_{OC} determined from difference of $R(V_{CELL-A})$ and $R(V_{CELL-B})$ at V_{oc} .

L/W	$R(V_{AB})$ (Ω/cm^2)	R_{OC} (Ω/cm^2)	FF(V_{CELL-A}) (%)
0.5	2.9	2.7	64
2.1	5.8	6.0	60
3.5	9.5	10	56

Figure 5 shows the two resistances plotted against L/W for devices on the same strip of Asahi SnO_2 . R_{OC} is the difference in R_{OC} for JV measured as V_{CELL-A} and V_{CELL-B} while $R(V_{AB})$ is the resistance obtained directly from the slope of V_{AB} as in Figure 4. Clearly, they are the same, verifying equations 2-4 that the difference in resistance between $R(V_{CELL-A})$ and $R(V_{CELL-B})$ is the same as $R(V_{AB})$, i.e., the TCO sheet resistance and TCO/p contact resistances. From the slope, R_{SH} is $\sim 8 \Omega/\text{sq}$ and from the intercept, $R_{TCO/p}$ is $2 \Omega/\text{cm}^2$.

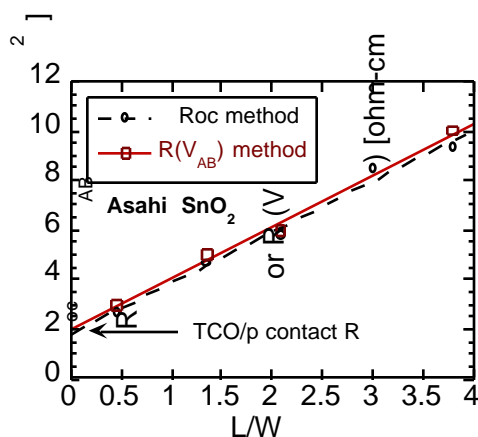


Figure 5. Resistance calculated from two methods vs L/W for row of cells on Asahi SnO_2 . The slope is the SnO_2 sheet resistance and the intercept is the TCO/p contact resistance.

Table III. TCO sheet resistance before and after a-Si deposition and TCO/p contact resistance for three types of SnO_2 . R_{SH} before deposition obtained from 4 point probe measurements.

TCO	R_{SH} (Ω/sq) before a-Si	R_{SH} (Ω/sq) after a-Si	$R_{TCO/p}$ (Ω/cm^2)
Solarex	~ 12	9	2.5
Asahi	~ 12	8	2.0
AFG	~ 13	9	2.5

Table III shows results from the 3 brands of SnO_2 studied. It indicates the SnO_2 sheet resistance is lower after a-Si deposition, with the largest change being for the Asahi SnO_2 . This decrease in SnO_2 sheet resistance is consistent with results from devices deposited at IEC on unscrubbed 1 inch squares of Asahi TCO. A tab-to-tab SnO_2 sheet resistance of 8-9 Ω/sq is typically found after fabrication of a device while the sheet resistance is 13-14 Ω/sq before deposition. The Asahi group has reported a decrease in SnO_2 resistivity of the same amount (from 12 to 8 Ω/sq)

with mild H₂ plasma treatments at 200°C due to increased mobility without any loss in optical transmission (9). Our results from Table III are consistent with these values.

Table III indicates a TCO/p contact resistance of approximately 2 Ω -cm² for all three SnO₂ materials. This value also includes any fixed contact or bulk parasitic resistances not accounted for in equations 2-4. However, values of ~1-2 Ω -cm² are reported by others (7,10) using special test structures (not p-i-n devices) which confirms that the values in Table III are representative of the TCO/p contact.

CONCLUSIONS

A new procedure has been presented to determine the TCO sheet resistance and TCO/p contact resistance in operating TCO/p-i-n superstrate devices. Devices must be fabricated on scribed TCO regions. Two independent methods give very close agreement, verifying the assumptions and analysis. Three brands of SnO₂ were studied here. Very similar TCO/p contact resistances were found. The sheet resistance of the Asahi brand SnO₂ decreased ~50% with a-Si processing. This is consistent with reports of others. We conclude that this technique can be helpful in evaluating factors which affect the TCO/p contact resistance, such use of new TCO materials or p-layer processing. In particular, it should be useful in solving the ZnO/p contact problem and evaluating the effect of microcrystalline p-layers.

ACKNOWLEDGMENTS

This work was supported under NREL subcontracts #ZAK-8-17619-33 and #ZAK-8-17619-02. We appreciate technical assistance from Ron Dozier in setting up the JV measurements.

REFERENCES

1. H. Shade, Z. Smith, J. Thomas, A. Catalano, *Thin Solid Films* **117**, 1984., p. 149.
2. S. Hegedus, H. Liang, R. Gordon, *AIP Proc.* **353**, 1995, p. 465.
3. R. Gordon, *Mat. Res. Soc. Symp. Proc.* **426**, 1996, p. 419.
4. L. Yang, M. Bennett, L. Chen, K. Jansen, J. Kessler, Y. Li, J. Newton, K. Rajan, F. Willing, R. Arya, D. Carlson, *Mat. Res. Soc. Symp. Proc.* **426**, 1996, p. 3.
5. P. Gerhardinger, R. McCurdy, *Mat. Res. Soc. Symp. Proc.* **426**, 1996, p. 399
6. S. Hegedus, W. Buchanan, X. Liu, R. Gordon, *Proc. 25th IEEE PVSC*, 1996, p. 1129.
7. M. Kubon, N. Shultz, M. Kolter, C. Beneking, H. Wagner, *Proc. 12th Euro. PVSEC*, 1994, p. 1268.
8. W. Shafarman and J. Phillips, *Proc. 25th IEEE PVSC*, 1996, p. 917.
9. K. Sato, Y. Gotoh, Y. Hayashi, H. Nishimura, *Proc. 21st IEEE PVSC*, 1990, p. 1584.
10. S. Guse, D. Peros, M. Wagner, M. Bohm, *Mat. Res. Soc. Symp. Proc.* **426**, 1996, p. 437.